

RSC Advances



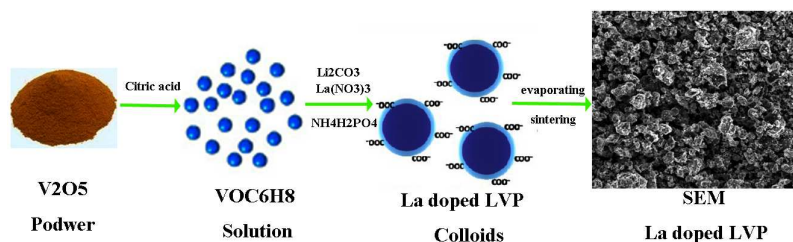
This is an *Accepted Manuscript*, which has been through the Royal Society of Chemistry peer review process and has been accepted for publication.

Accepted Manuscripts are published online shortly after acceptance, before technical editing, formatting and proof reading. Using this free service, authors can make their results available to the community, in citable form, before we publish the edited article. This *Accepted Manuscript* will be replaced by the edited, formatted and paginated article as soon as this is available.

You can find more information about *Accepted Manuscripts* in the [Information for Authors](#).

Please note that technical editing may introduce minor changes to the text and/or graphics, which may alter content. The journal's standard [Terms & Conditions](#) and the [Ethical guidelines](#) still apply. In no event shall the Royal Society of Chemistry be held responsible for any errors or omissions in this *Accepted Manuscript* or any consequences arising from the use of any information it contains.

Graphical Abstract



The La-doped $\text{Li}_3\text{V}_2(\text{PO}_4)_3/\text{C}$ cathode materials are synthesized by a sol-gel-assisted, low-temperature sintering process. The resulting $\text{Li}_3\text{V}_{1.96}\text{La}_{0.04}(\text{PO}_4)_3/\text{C}$ cathode has a stable specific capacity of 160 mAh g^{-1} at low charge–discharge rates over 100 cycles, and retained a stable capacity of up to 116 mAh g^{-1} at a rate of 5C, which is 40% higher than the undoped pristine cathode.

Sol-Gel-Assisted, Fast and Low-Temperature Synthesis of La-doped $\text{Li}_3\text{V}_2(\text{PO}_4)_3/\text{C}$ Cathode Materials for Lithium-Ion Batteries

Zhenyu Yang^{1,*}, Jinhua Hu¹, Zhengyu Chen¹, Jing Zhong², Ningyu Gu^{1,*} and Ning Zhang¹

¹Department of Chemistry, Nanchang University, No.999, Xuefu Road, New District of Honggutan, Nanchang, Jiangxi, 330031, P. R. China

²School of Civil Engineering, Harbin Institute of Technology, Heilongjiang 150090, P. R. China

*Corresponding authors: zyyang@ncu.edu.cn, nygu@ncu.edu.cn

ABSTRACT:

A series of La-doped $\text{Li}_3\text{V}_2(\text{PO}_4)_3/\text{C}$ cathode materials for Li-ion batteries are synthesized by a sol-gel-assisted, low-temperature sintering process. $\text{La}(\text{NO}_3)_3$ acts not only as the La source, but also, together with the intermediate product LiNO_3 , promotes combustion, the ultrahigh exothermic energy that is advantageous for the nucleation process. The subsequent sintering process at 600 °C for 4 h is sufficient to produce highly crystalline La-doped $\text{Li}_3\text{V}_2(\text{PO}_4)_3/\text{C}$ composites. The as-prepared cathode materials display smaller particle size, lower electron-transfer resistance and faster Li ion migration, which is ascribed to enhanced Li-ion transfer because of the La doping. The resulting $\text{Li}_3\text{V}_{1.96}\text{La}_{0.04}(\text{PO}_4)_3/\text{C}$ cathode has a stable specific capacity of 160 mAh g⁻¹ at low charge–discharge rates over 100 cycles, and retained a stable capacity of up to 116 mAh g⁻¹ at a rate of 5C, which is 40% higher than the undoped pristine cathode.

Keywords: La-doped, $\text{Li}_3\text{V}_2(\text{PO}_4)_3/\text{C}$, composite, promoter, cathode, Li-ion battery

1. Introduction

As an electrochemical energy storage devices, Li-ion batteries(LIBs) have been widely used in wireless telephones, laptop computers, digital cameras, and other electronic devices since they were first introduced in the 1990s [1, 2]. Recently, the application of LIB technology in electrical energy storage systems for smart grids that are powered by conventional energy sources such as coal, as well as intermittent renewable energy sources such as solar and wind, has attracted considerable attention.

In the present LIB market, any Li-ion cathode needs to satisfy the demands of high energy density, fast charging capability, long shelf-life and safety. To address these requirements, great efforts have been made to develop phosphate-based cathodes because the strongly covalent $(\text{PO}_4)^{3-}$ units provide greater structural stability than commercial LiCoO_2 hosts even under deep charging conditions and elevated temperatures[3-6].

Among the known phosphates, monoclinic $\text{Li}_3\text{V}_2(\text{PO}_4)_3$ (LVP) is a promising LiB cathode because of its higher operating voltage (~ 4.8 V) and its ability to deliver a capacity of 197 mAh g^{-1} as 3 Li-ions are inserted/extracted in the operating voltage range of 3.0–4.8 V [7-14]. However, monoclinic LVP suffers from low electrical conductivity ($\sim 2.4 \times 10^{-8} \text{ S cm}^{-1}$); hence, achieving its full theoretical capacity and a high rate performance is challenging. The majority of the strategies to overcome these obstacles are focused on doping with metal ions [15-27], coating with carbon [29-31] or scaling down the LVP particle size [32-36]. Up to now, lots of elements have been extensively investigated, such as alkali metals(Na) [28], alkaline-earth metals (Mg)

[10, 37], transition metals (Ti, Cr, Mn, Fe, Co, Ni, Zr, Nb, Mo, Zn) [15-27], main group element metals (Al, Sn, Ge) [22, 24], and halogens (Cl, F) [38]. Relative to them, there are few works involving the study of the substitution behavior of lanthanide element (Ce, Nd, and Sm) [23, 39] in the vanadium site in LVP systems. Yao et. Al. [9] prepared the Ce-doped $\text{Li}_3\text{V}_{2-x}\text{Ce}_x(\text{PO}_4)_3/\text{C}$ composites by a sol-gel method and the $\text{Li}_3\text{V}_{2-x}\text{Ce}_x(\text{PO}_4)_3/\text{C}(x=0.05)$ exhibited the best rate and cycle performance. Dang et. al. [19] also synthesis the Ce-doped $\text{Li}_3\text{V}_{2-x}\text{Ce}_x(\text{PO}_4)_3/\text{C}$ composites by a microwave assisted sol-gel process, and electrochemical performance measurements exhibited that $\text{Li}_3\text{V}_{1.98}\text{Ce}_{0.02}(\text{PO}_4)_3/\text{C}$ exhibited a good cycling performance, with a retention rate of discharge capacity of 94 % at 0.2 C after 100 cycles. In addition, Tm-doped $\text{Li}_3\text{V}_{2-x}\text{Tm}_x(\text{PO}_4)_3/\text{C}$ samples prepared by solid-state reaction could deliver discharge capacity of 181 mAh g^{-1} at 0.1C and sustain 95% of capacity retention after 20 cycles [40]. Although many kinds of doped $\text{Li}_3\text{V}_2(\text{PO}_4)_3$ have been studied, the electrochemical performance of the composite electrode has not yet reached a satisfactory level.

Lanthanum (La) has a relatively large radius and high affinity for oxygen, and La-doping can enhance the superconductivity and stability of materials [41]. La is the second most abundant rare earth element in the world (32 ppm in Earth's crust) and it is inexpensive (e.g. lanthanum ammonium nitrate, 99.9%, \$1.93 per pound, Lindsay Chem., USA), making it attractive for large-scale commercial applications. It is noted that the La-doped $\text{Li}_3\text{V}_{2-x}\text{La}_x(\text{PO}_4)_3$ samples have been synthesized by Jiang et al. using lanthanum oxide (La_2O_3) as the La source. The $\text{Li}_3\text{V}_{2-x}\text{La}_x(\text{PO}_4)_3$ ($x = 0.02$)

sample showed the highest discharge capacity of 168 mAh g^{-1} at 0.2C rate in the potential range of 3.0–4.8 V, with a retention rate of discharge capacity of 93 % at 0.2 C after 30 cycles[42]. On the basis of this, we prepared the La-doped carbon coating $\text{Li}_3\text{V}_2(\text{PO}_4)_3$ composite materials using a low temperature and fast sol-gel method with spontaneous chemical reactions in the present study. The low reaction temperature and the short reaction time are made possible because of the selection of $\text{La}(\text{NO}_3)_3$ and the intermediate product of LiNO_3 , both of which promote combustion, the ultrahigh exothermic energy of which accelerates the nucleation process. The effects of La substitution on the electrochemical properties and rate performance of as-obtained $\text{Li}_3\text{V}_2(\text{PO}_4)_3/\text{C}$ composites are investigated in detail.

2. Experiment

The $\text{Li}_3\text{V}_{2-x}\text{La}_x(\text{PO}_4)_3/\text{C}$ cathode materials ($x=0, 0.02, 0.04, 0.06$) were synthesized by a low-temperature and fast sol-gel route in a molar ratio of Li: V: La :P = 3: 2–x: x: 3 using Li_2CO_3 , V_2O_5 , $\text{La}(\text{NO}_3)_3$ and $\text{NH}_4\text{H}_2\text{PO}_4$ as raw materials as shown in Fig 1. All chemicals used in this work were analytical grade without any pre-treatment. Firstly, V_2O_5 and citric acid were dissolved in deionized water at 70°C to form VOC_6H_8 solution. Then, the mixed Li_2CO_3 , $\text{La}(\text{NO}_3)_3$ and $\text{NH}_4\text{H}_2\text{PO}_4$ solution was added into the prepared VOC_6H_8 solution with magnetic stirring to form brown LVP hydrophilic homogeneous colloids with anionic surface. In order to chelate the metal ions uniformly by citric acid, the pH value of above solution was adjusted to about 8.0~9.0 using $\text{NH}_3\cdot\text{H}_2\text{O}$. Subsequently, the colloids solution was heated to $\sim 80^\circ\text{C}$ for

~6 hours under active stirring for the purpose of evaporating the water until the gel was formed. Next, the precursor was obtained after drying at ~80°C for ~24 hours in an oven. Afterwards, the obtained precursor was carefully grounded after cooling to room temperature, and was sintered at 600 °C for ~4 hours in flowing N₂ to yield the La-doping Li₃V_{2-x}(PO₄)₃/C composite (x=0, 0.02, 0.04, 0.06, 0.08).

X-ray diffraction patterns were obtained using an Philips X'Pert diffractometer with Cu K_α radiation. Thermogravimetric (TG) analysis was performed by using a SDTA851E thermoanalyzer using a heating rate of 10 °C·min⁻¹. The morphology was obtained with a field-scanning electron microscope (SEM, JSM-6390LA) and a transmission electron microscope ((TEM, JEOL JEM- 200CX, 200 kV).

Electrochemical properties were evaluated with model CR2025 coin-type cell. The working electrodes were prepared as follows: a mixture of 82 wt% active materials, 10 wt% carbon black, and 8 wt% polyvinylidene fluoride (PVDF) binder in N-methylpyrrolidinone was create a slurry. The resulting slurry was coated on an Al current collector with a thickness of ~75 μm. The cathodes were dried in a vacuum furnace at 65°C for ~20 hours, following which they were roll-pressed at a pressure of ~15 MPa. Circular electrodes (12 mm in diameter) were then punched out. The typical weight of the cathode ranged from ~7 to 8 mg. Finally, the cathode was dried again in a vacuum oven at ~100°C for ~48 hours prior to assembly. The cells were assembled in a high purity argon atmosphere inside a glove box (Mbraunlab Master130, Germany). Celgard® 2325 was used as the separator and the electrolyte was a solution of 1M LiPF₆ dissolved in a mixture of ethylene carbonate (EC):

dimethyl carbonate (DMC) (1:1vol.%). The cells were cycled at different rates between 3.0 and 4.8 V on a cell testing instrument(LAND CT2001A, China). Electrochemical impedance spectra (EIS) measurements were performed on an electrochemical working station (PARSTAT2273, Princeton Applied Research, U.S.). EIS spectra were obtained over a frequency range between 1 mHz and 100 kHz.

3 Results and discussion

The thermogravimetric (TG) curves for the dry gel precursors of $\text{Li}_3\text{V}_{2-x}\text{La}_x(\text{PO}_4)_3/\text{C}$ ($x = 0, 0.02, 0.04, 0.06$) are shown in Fig. 2. The data were acquired in the temperature range from 25°C to 800 °C at a heating rate of ~10 °C /min under N_2 flow. Similar curves were obtained for all dry gel precursors. Approximately ~40.6% weight loss is observed for the dry gel precursor of $\text{Li}_3\text{V}_{1.96}\text{La}_{0.04}(\text{PO}_4)_3/\text{C}$ in the temperature sweep to ~600 °C, above which the weight loss is insignificant. In the TG curves, there are three main weight loss stages: below 200 °C, 200-450 °C and 450-600 °C. The 13.9% weight just below ~200 °C is attributed to loss of crystalline water, absorbed water, ammonia and hydrogen fluoride. From 200 to 450 °C, the weight loss is approximately 18.5 wt%, which is owing to the pyrolysis of citric acid. From 450 to 600 °C, the weight loss is approximately ~8.2%, which can be attributed to the pyrolysis of the remaining organic compounds. As previously mentioned, there was no significant weight loss observed in the TG curve above 600 °C, which indicates that the stable composites of La-doped $\text{Li}_3\text{V}_2(\text{PO}_4)_3/\text{C}$ composites are formed and that the chemical reactions had reached completion.

On the base of the TG analysis, the La-doped $\text{Li}_3\text{V}_2(\text{PO}_4)_3/\text{C}$ composites were prepared by a sol-gel method at $\sim 600^\circ\text{C}$ for ~ 4 h. The low reaction or sintering temperature and the short reaction time are made possible by the selection of $\text{La}(\text{NO}_3)_3$ and the intermediate product of LiNO_3 . Because of these molecules are combustion promoters, a large amount of energy will be released during the reaction, which is advantageous for the nucleation process.

The XRD experiments were conducted to investigate the structural changes caused by incorporation of different concentration of La ions in the $\text{Li}_3\text{V}_{2-x}\text{La}_x(\text{PO}_4)_3/\text{C}$ ($x=0, 0.02, 0.04, 0.06$) samples. As shown in Fig.3, the XRD patterns of the $\text{Li}_3\text{V}_{2-x}\text{La}_x(\text{PO}_4)_3/\text{C}$ samples are similar to that of the undoped sample. No impurity phases are detectable at the resolution of the X-ray diffractometer. This confirms that La ion are doped into the crystalline structure of $\text{Li}_3\text{V}_2(\text{PO}_4)_3$. The typical monoclinic structure can be indexed with the space group $\text{P}2_1/\text{n}$ (ICSD #96962, #01-072-7074) by all fundamental peaks [43], which suggests that La was successfully incorporated into the $\text{Li}_3\text{V}_2(\text{PO}_4)_3/\text{C}$ crystal lattice, and the basic crystal structure of $\text{Li}_3\text{V}_2(\text{PO}_4)_3/\text{C}$ is unchanged. Accordingly, the unit cell lattice parameters of all the samples have been refined, and are shown in Table 1. An increase in the unit cell volume is caused by the replacement of V by La in the monoclinic structure, which is consistent with the fact that the radius of V^{3+} in the VO_6 octahedra is smaller than La^{3+} . The cell parameters of the $\text{Li}_3\text{V}_2(\text{PO}_4)_3/\text{C}$ sample also agree well with those reported in the literature [44]. The previous studies differ from the present study only in terms of the different carbon sources(e. g. humic acid, glucose) and synthesis methods. The results indicate

that in the crystal lattice, La ions are positioned in the V^{3+} sites, and the crystallinity of $Li_3V_2(PO_4)_3$ is retained even after La doping. This high crystallinity of $Li_3V_2(PO_4)_3$ is a critical factor that can significantly improve the cycling stability of the $Li_3V_2(PO_4)_3$ cathode[45].

The carbon content of the $Li_3V_{2-x}La_x(PO_4)_3/C$ ($x = 0, 0.02, 0.04, 0.06$) samples was determined from elemental analysis to be $\sim 8.14\%$, $\sim 9.37\%$, $\sim 8.29\%$, and $\sim 8.18\%$, respectively (not shown here). Such a high carbon content is critical for keeping an effective electrical contact between particles [31]. However, no corresponding peaks were detected by the XRD spectra (Fig. 3), which could be associated with the fact that the residual carbon is amorphous in the $Li_3V_{2-x}La_x(PO_4)_3/C$ composites [46]. Consequently, the presence of the amorphous carbon does not affect the $Li_3V_{2-x}La_x(PO_4)_3/C$ crystalline structure, and improves the mechanical stability and the electronic conductivity of the $Li_3V_2(PO_4)_3$ materials.

Scanning electron microscopy (SEM) images of the La-doped and undoped $Li_3V_2(PO_4)_3 /C$ samples are shown in Fig. 4. All the powders show flake-like surface profiles. The $Li_3V_2(PO_4)_3/C$ particles are less than $1\mu m$ in diameter and slightly agglomerated as displayed in Fig.4(A). Thus, the $Li_3V_{1.96}La_{0.04}(PO_4)_3/C$ composite has the most uniform morphology and small particle size (i.e. highest specific surface area) of the three doped samples. Such a microstructure will serve to shorten the Li ion diffusion distance from the cathode bulk phase to the electrolyte and facilitate the electrolyte penetration, thereby ensuring better wettability. The high-resolution transmission electron microscopy (HRTEM) image of the composites

are shown in Fig. 5. It can be seen that there is an amorphous carbon layer (~5-8 nm thick) on the $\text{Li}_3\text{V}_{1.96}\text{La}_{0.04}(\text{PO}_4)_3$ surface. Such an amorphous carbon network can facilitate better inter-particles electronic contact, and, as a result, reduce the inter-particle contact resistance and improve the electrochemical properties of the composites.

To determine the electrochemical properties of the composites, the charge-discharge characteristic were measured at constant current density. The initial charge-discharge curves of pristine and La-doped $\text{Li}_3\text{V}_{2-x}\text{La}_x(\text{PO}_4)_3/\text{C}$ ($x = 0.02, 0.04, 0.06$) composites at a charge/discharge rate (C-rate) of ~0.2C between 3.0 V and 4.8 V are shown in Fig. 6. All composites display four voltage plateaus during the charging process at approximately ~3.60, ~3.70, ~4.10 and ~4.60 V, and during the discharging process, there are three voltage plateaus at approximately ~3.56, ~3.65, and ~4.1V. These results indicate a sequence of phase transition processes taking place in the $\text{Li}_x\text{V}_2(\text{PO}_4)_3$ ($x = 3.0, 2.5, 2.0, 1.0$), respectively [19]. It is also apparent that the initial discharge capacities of the $\text{Li}_3\text{V}_{2-x}\text{La}_x(\text{PO}_4)_3/\text{C}$ samples are dependent on the La-doping amounts. The charge capacities of $\text{Li}_3\text{V}_{2-x}\text{La}_x(\text{PO}_4)_3/\text{C}$ composites ($x = 0, 0.02, 0.04, 0.06$) are approximately ~175, ~180, ~179, and ~181 mAh g^{-1} , respectively; the discharging capacities are approximately ~161, ~168, ~171 and ~164 mAh g^{-1} , respectively. The coulombic efficiencies of these composites are approximately ~91%, ~93%, ~95%, and ~92%, respectively. The high coulombic efficiencies of these composites are indicative of reversible phase transformations in the monoclinic $\text{Li}_3\text{V}_{2-x}\text{La}_x(\text{PO}_4)_3/\text{C}$ composites, which correspond to lithiation and

delithiation steps, and accordingly lead to reversibility during continuous cycling [47]. It is noted that the discharge capacity is improved considerably when the La ion doping level is $x=0.04$. The high specific discharge capacity of $\text{Li}_3\text{V}_{1.96}\text{La}_{0.04}(\text{PO}_4)_3/\text{C}$ could arise because of a decrease of grain size and favorable homogeneity (as shown in Fig. 4). Figure 7 shows the cycling performance of $\text{Li}_3\text{V}_{2-x}\text{La}_x(\text{PO}_4)_3/\text{C}$ composites ($x = 0, 0.02, 0.04, 0.06$) in the voltage range of 3.0-4.8V at a rate of 0.2C rate. The discharge capacity retention is ~84%, ~91%, ~94%, and ~89% after 100 cycles for the $\text{Li}_3\text{V}_{2-x}\text{La}_x(\text{PO}_4)_3/\text{C}$ ($x= 0, 0.02, 0.04, 0.06$) composites, respectively. These results demonstrate that La doping considerably improves the cycling stability of $\text{Li}_3\text{V}_2(\text{PO}_4)_3$, with the optimum doping level being $x= 0.04$. The enhanced cycling stability will be explained by the structure of $\text{Li}_3\text{V}_2(\text{PO}_4)_3/\text{C}$ being stabilized by La-doping. To summarize, $\text{Li}_3\text{V}_{1.96}\text{La}_{0.04}(\text{PO}_4)_3/\text{C}$ demonstrates the most promising electrochemical performance of all the composites as tested, exhibiting both high initial capacity and capacity retention. More details about the effect of the various lanthanide ion doping on the electrochemical performance of $\text{Li}_3\text{V}_2(\text{PO}_4)_3/\text{C}$ cathodes are listed in Table 2. It can be found that the La doping system in this work have promising performance among these lanthanide ion-doped systems.

Figure 8 shows the contrast in the rate performance between the undoped pristine and La-doped $\text{Li}_3\text{V}_{1.96}\text{La}_{0.04}(\text{PO}_4)_3/\text{C}$ composites. It can be seen that the undoped pristine $\text{Li}_3\text{V}_2(\text{PO}_4)_3/\text{C}$ material can delivers a specific capacity of $\sim 153 \text{ mAhg}^{-1}$ at a rate of $\sim 1\text{C}$. When the C-rate is increased from $\sim 1\text{C}$ to $\sim 2\text{C}$, the specific capacity retains $\sim 86\%$. For the La-doped $\text{Li}_3\text{V}_{1.96}\text{La}_{0.04}(\text{PO}_4)_3/\text{C}$ composite, a specific capacity

of $\sim 162 \text{mAhg}^{-1}$ is obtained at a rate of $\sim 1\text{C}$, which drops to $\sim 93\%$ ($\sim 148 \text{mAhg}^{-1}$) when the rate is increased $\sim 2\text{C}$. When the rate is increased from $\sim 2\text{C}$ to $\sim 5\text{C}$, the difference in the specific capacity between the pristine and La doped composites becomes pronounced. For the La-doped $\text{Li}_3\text{V}_{1.96}\text{La}_{0.04}(\text{PO}_4)_3/\text{C}$ composites, the specific capacity is $\sim 116 \text{mAh g}^{-1}$ ($\sim 70\%$) at 5C , whereas that of the undoped pristine sample is only $\sim 82.0 \text{mAh g}^{-1}$ ($\sim 50\%$). It is also noted that the specific capacity of the $\text{Li}_3\text{V}_{1.96}\text{La}_{0.04}(\text{PO}_4)_3/\text{C}$ composites recovers to $\sim 159 \text{mAhg}^{-1}$ ($\sim 94\%$) when the C-rate is returned back to 1C from 5C , whereas that of the undoped pristine $\text{Li}_3\text{V}_2(\text{PO}_4)_3/\text{C}$ recovers to only $\sim 138 \text{mAhg}^{-1}$ ($\sim 83\%$). The high-rate performance of $\text{Li}_3\text{V}_{1.96}\text{La}_{0.04}(\text{PO}_4)_3/\text{C}$ composites is attributed to faster Li ion migration, more uniform particle distribution via the sol-gel method and the low-temperature sintering process with spontaneous chemical reactions. The above results demonstrate that at the higher rates (5C), the electrochemical dynamics for the $\text{Li}_3\text{V}_{1.96}\text{La}_{0.04}(\text{PO}_4)_3/\text{C}$ composites are influenced by the Li ion diffusion in the bulk material rather than only by the electrochemical reaction rate.

The kinetic properties of $\text{Li}_3\text{V}_{1.96}\text{La}_{0.04}(\text{PO}_4)_3/\text{C}$ can be further analyzed by electrochemical impedance spectroscopy (EIS). Figure 9 shows the Nyquist plots for the $\text{Li}_3\text{V}_2(\text{PO}_4)_3/\text{C}$ and $\text{Li}_3\text{V}_{1.96}\text{La}_{0.04}(\text{PO}_4)_3/\text{C}$ electrodes. The inset equivalent circuit is used to simulate the impedance spectra. The low-frequency semicircle shows the Li-ion diffusion in the bulk of the electrode and the process is related to the Warburg impedance (W_1). The middle frequency is associated with the charge-discharge process, which includes charge transfer resistance (R_1), the particle-to-particle

resistance(R_2), the double-layer capacitance (CPE_1) and the capacitance at the electrode-electrolyte interface(CPE_2). The high frequencies are attributed to the interfacial resistance on the electrodes and the intercept corresponds to the electrolyte resistance (R_e). As seen in Fig. 9, the charge-transfer resistance of the $\text{Li}_3\text{V}_{1.96}\text{La}_{0.04}(\text{PO}_4)_3/\text{C}$ composite ($\sim 187 \Omega$) is significantly lower than that of the $\text{Li}_3\text{V}_2(\text{PO}_4)_3/\text{C}$ composite ($\sim 294 \Omega$), which is likely because of the increase in electron conductivity that results from La-doping. In the impedance spectra, the low impedance values are related to the diffusion of Li ions (low-frequency spike) in the $\text{Li}_3\text{V}_{1.96}\text{La}_{0.04}(\text{PO}_4)_3/\text{C}$ composites. The low impedance is associated with higher surface area, uniform particle size distribution and better electrolyte wettability. This may be related to the use of $\text{La}(\text{NO}_3)_3$ and the intermediate product of LiNO_3 in the sintering process. As discussed earlier, these molecules promote combustion, the ultrahigh exothermic energy of which accelerates the nucleation reaction. These factors results in greater accessibility to active sites for the Li ions, faster Li ion diffusion, shorter diffusion distances, and, consequently, improve the rate performance of the $\text{Li}_3\text{V}_{1.96}\text{La}_{0.04}(\text{PO}_4)_3/\text{C}$ electrode.

4. Conclusions

$\text{Li}_3\text{V}_2(\text{PO}_4)_3/\text{C}$ and La-doped $\text{Li}_3\text{V}_2(\text{PO}_4)_3/\text{C}$ composites were synthesized by a sol-gel-assisted, low-temperature sintering process. $\text{La}(\text{NO}_3)_3$ acted not only as the La source, but also, together with the intermediate product of LiNO_3 , promoted combustion, which accelerated the nucleation process. We analyzed the influence of

La doping on the electrochemical performance and structural characteristics of $\text{Li}_3\text{V}_2(\text{PO}_4)_3/\text{C}$. The results demonstrated that La could be incorporated into the crystal structure of $\text{Li}_3\text{V}_2(\text{PO}_4)_3/\text{C}$ and the as-prepared cathode materials had smaller particle sizes, faster Li ion migration kinetics, and lower electron-transfer resistance. The $\text{Li}_3\text{V}_{1.96}\text{La}_{0.04}(\text{PO}_4)_3/\text{C}$ cathode had a stable specific capacity of $\sim 160 \text{ mAhg}^{-1}$ at low charge-discharge rates over 100 cycles, and the cathode could still attain a stable capacity of up to $\sim 116 \text{ mAhg}^{-1}$ at a rate of 5C rates (40% higher than its undoped pristine cathode).

Acknowledgments

Z. Yang and N. Gu acknowledges funding support by the National Natural Science Foundation of China (Grant No. 20963007, 21263016, 21363015).

References

- [1] M. Armand, J. M. Tarascon, *Nature*, 2008, 451, 652.
- [2] L. Shen, H. Li, E. Uchaker, *Nano Lett.*, 2012, **12**, 5673.
- [3] R. Mukherjee, A. V. Thomas, N. Koratkar, *ACS Nano*, 2012, **6**, 7867.
- [4] R. Mukherjee, A. V. Thomas, E. Singh, *Nature Communications* 2014, **5**, 3710.
- [5] J. W. Kang, V. Mathew, J. Gim, *Sci. Rep.*, 2014, **4**, 4047.
- [6] W. Xu, L. Liu, H. Guo, R. Guo, *Electrochimica Acta*, 2013, **113**, 497.
- [7] A. Pan, D. Choi, J. G. Zhang, S. B. Arey, *J. Power Sources*, 2011, **196**, 3646.
- [8] Y. Q. Qiao, X. L. Wang, Y. J. Mai, *J. Power Sources*, 2011, **196**, 8706.
- [9] J. Yao, S. Wei, P. Zhang, L. Wang, *J. Alloys. Compounds*, 2012, **532**, 49.
- [10] C. Dai, Z. Chen, H. Jin, X. Hu, *J. Power Sources*, 2010, **195**, 5775.
- [11] A. K. Padhi, K. S. Nanjundaswamy, J. B. Goodenough, *J. Electrochem. Soc.*, 1997, **144**, 1188.
- [12] M. Y. Saidi, J. Barker, H. Huang, J. L. Swoyer, G. Adamson, *Electrochem. Solid-State Letters*, 2002, **5**, A149.
- [13] W. Yuan, J. Yan, Z. Tang, O. Sha, J. Wang, *Electrochim. Acta* 2012, **72**, 138.

- [14] D. Ai, K. Liu, Z. Lu, M. Zou, D. Zeng, *Electrochim. Acta* 2011, **56**, 2823.
- [15] M. Ren, Z. Zhou, Y. Li, X. P. Gao, J. Yan, *J. Power Sources* 2006, **162**, 1357.
- [16] Y. Z. Dong, Y. M. Zha, H. Duan, *J. Electroanal. Chem.* 2011, **660**, 14.
- [17] T. Jiang, Y. J. Wei, W. C. Pan, Z. Li, *J. Alloys Compounds*, 2009, **488**, L26.
- [18] Y. H. Chen, Y. M. Zhao, X. N. An, *Electrochimica Acta*, 2009, **54**, 5844.
- [19] J. Dang, F. Xiang, N. Gu, R. Zhang, *J. Power Sources* 2013, **243**, 33.
- [20] S. Y. Yang, S. Zhang, B. L. Fu, Q. Wu, F. L. Liu, *J. Solid State Electrochem.*, 2012, **15**, 2633.
- [21] C. Deng, S. Zhang, S. Y. Yang, Y. Gao, *J. Phys. Chem. C*, 2011, **115**, 15048.
- [22] H. Liu, S. Bi, G. Wen, X. Teng, *J. Alloys and Compounds*, 2012, **543**, 99.
- [23] Y. Xia, W. Zhang, H. Huang, Y. Gan, *Materials Science and Engineering: B*, 2011, **176**, 663.
- [24] A. R. Cho, J. N. Son, V. Aravinda, H. Kim, *J. Mater. Chem.*, 2012, **22**, 6556.
- [25] J. N. Sona, G. J. Kim, M. C. Kim, S. H. Kim, V. Aravindana, *J. Electrochem. Soc.*, 2013, **160**, A87.
- [26] W. Wang, J. Zhang, Z. Jia, C. Dai, *Phys. Chem. Chem. Phys.*, 2014, **16**, 13858.
- [27] S. Zhang, Q. Wu, C. Deng, F. L. Liu, *J. Power Sources*, 2012, **218**, 56.
- [28] Q. Kuang, Y. Zhao, Z. Liang, *J. Power Sources*, 2011, **196**, 10169.
- [29] Y. Q. Qiao, J. P. Tu, X. L. Wang, C. D. Gu, *J. Power Sources*, 2012, **199**, 287
- [30] Y. Q. Qiao, J. P. Tu, X. L. Wang, *J. Power Sources*, 2011, **196**, 7715
- [31] M. Koltypin, V. Pol, A. Gedanken, D. Aurbach, *J. Electrochem. Soc.* 2007, **154**, A605
- [32] L. Mai, L. Xu, C. Han, X. Xu, *Nano Lett.* 2010, **10**, 4750.
- [33] Y. Q. Qiao, J. P. Tu, Y. J. Mai, *J. Alloys Compounds*, 2011, **509**, 7181
- [34] H. Liu, P. Gao, J. Fang, G. Yang, *Chemical Communications*, 2011, **47**, 9110
- [35] Q. Q. Chen, T. T. Zhang, X. C. Qiao, D. Q. Li, *J. Power Sources*, 2013, **234**, 197
- [36] G. Zhang, X. Li, H. Jia, X. Pang, *Int. J. Electrochem. Sci.*, 2012, **7**, 830.
- [37] J. S. Huang, L. Yang, K. Y. Liu, Y. F. Tang, *J. Power Sources*, 2010, **195**, 5013.
- [38] J. Yan, W. Yuan, Z. Y. Tang, *J. Power Sources*, 2012, **209**, 251.
- [39] S. Wang, Z. Zhang, A. Deb, L. Yang, S. Hirano, *Ind. Eng. Chem. Res.*, 2014, **53**, 19525.
- [40] X. Yang, L. Jun, H. Jia, *Electrochimica Acta*, 2014, **50**, 62.
- [41] X. Lin, X. Ni, B. Chen, X. Xu, X. Yang, *Phys. Rev. B*, 2013, **87**, 20504.
- [42] B. Jiang, S. Hu, M. Wang, X. Ouyang, *Rare Metals*, 2011, **30**, 115.
- [43] Q. Wei, Q. An, D. Chen, L. Mai, *Nano Lett.* 2014, **14**, 1042.
- [44] X. Zhou, Y. Liu, Y. Guo, *Electrochimica Acta*, 2009, **54**, 2253.
- [45] H. C. Shin, W. I. Cho, H. Jang, *J. Power Sources*, 2006, **159**, 1383.
- [46] M. Y. Saidi, J. Barker, H. Huang, J. L. Swoyer, *J. Power Sources* 2003, **119**, 266.
- [47] W. Wang, H. Wang, S. Liu, *J. Solid State Electrochem.* 2012, **16**, 2555.

Caption of the Figures

Fig. 1. The processes of the La doped $\text{Li}_3\text{V}_2(\text{PO}_4)_3/\text{C}$ composites

Fig. 2. TG curve for the dry gel precursor of $\text{Li}_3\text{V}_{2-x}\text{La}_x(\text{PO}_4)_3/\text{C}$ ($x=0, 0.02, 0.04, 0.06$) under N_2 flow at a heating rate of $10^\circ\text{C}/\text{min}$.

Fig. 3. XRD patterns of the $\text{Li}_3\text{V}_{2-x}\text{La}_x(\text{PO}_4)_3/\text{C}$ ($x=0, 0.02, 0.04, 0.06$) samples as a function of La ion doping

Fig. 4 SEM images of $\text{Li}_3\text{V}_{2-x}\text{La}_x(\text{PO}_4)_3/\text{C}$ samples with different La contents: (a) $x=0$, (b) $x=0.02$; (c) $x=0.04$; (d) $x=0.06$;

Fig. 5 TEM images of $\text{Li}_3\text{V}_{1.96}\text{La}_{0.04}(\text{PO}_4)_3/\text{C}$.

Fig. 6 Initial charge-discharge profiles of $\text{Li}_3\text{V}_{2-x}\text{La}_x(\text{PO}_4)_3/\text{C}$ ($x=0, 0.02, 0.04, 0.06$) at the 0.2C rate in the voltage of 3.0V- 4.8V.

Fig. 7 Cycling performance of $\text{Li}_3\text{V}_{2-x}\text{La}_x(\text{PO}_4)_3/\text{C}$ ($x=0, 0.02, 0.04, 0.06$) at 0.2C discharge rate between 3.0V and 4.8V.

Fig. 8 Cycling performance of $\text{Li}_3\text{V}_2(\text{PO}_4)_3/\text{C}$ and $\text{Li}_3\text{V}_{1.96}\text{La}_{0.04}(\text{PO}_4)_3/\text{C}$ at different discharge rate of 0.2C, 1C, 2C, and 5C, respectively, between 3.0V-4.8V.

Fig. 9 Impedance spectra of the $\text{Li}_3\text{V}_2(\text{PO}_4)_3/\text{C}$ and $\text{Li}_3\text{V}_{1.96}\text{La}_{0.04}(\text{PO}_4)_3/\text{C}$ composites. Inset: Equivalent circuit corresponding to the impedance diagrams.

Table 1 Lattice parameters of $\text{Li}_3\text{V}_{2-x}\text{La}_x(\text{PO}_4)_3/\text{C}$ cells ($x=0,0.02,0.04,0.06$) samples and comparative data for $\text{Li}_3\text{V}_{2-x}\text{La}_x(\text{PO}_4)_3$ phase were taken from X. Zhou et al[44].

samples	a (nm)	b (nm)	c (nm)	β (°)	V (nm ³)
$\text{Li}_3\text{V}_2(\text{PO}_4)_3/\text{C}$	0.8602(4)	0.8594(2)	1.2042(5)	89.89	0.8896
$\text{Li}_3\text{V}_{1.98}\text{La}_{0.02}(\text{PO}_4)_3/\text{C}$	0.8611(3)	0.8596(5)	1.2061(4)	90.32	0.8924
$\text{Li}_3\text{V}_{1.96}\text{La}_{0.04}(\text{PO}_4)_3/\text{C}$	0.8620(3)	0.8601(4)	1.2076(3)	90.46	0.8953
$\text{Li}_3\text{V}_{1.94}\text{La}_{0.06}(\text{PO}_4)_3/\text{C}$	0.8624(5)	0.8597(2)	1.2095(4)	90.41	0.8967
$\text{Li}_3\text{V}_2(\text{PO}_4)_3$ ^[44]	0.8602	0.8585	1.2020	90.53	0.8878

Table 2 Comparative electrochemical performance data for the various lanthanide ion doped $\text{Li}_3\text{V}_2(\text{PO}_4)_3/\text{C}$ cathodes in 3.0-4.8 V.

Sample	Method	Electrochemical performance	Ref.
$\text{Li}_3\text{V}_{1.95}\text{Ce}_{0.05}(\text{PO}_4)/\text{C}$	Sol-gel reaction	In 3.0-4.8V, 120 mAhg^{-1} with 96.8% capacity retention after 100 cycles at 0.2C	9
$\text{Li}_3\text{V}_{1.98}\text{Ce}_{0.02}(\text{PO}_4)/\text{C}$	Microwave assisted Sol-gel reaction	In 3.0-4.8V, 171.6 mAhg^{-1} with 94.0% capacity retention after 100 cycles at 0.2C	19
$\text{Li}_3\text{V}_{1.97}\text{Ce}_{0.03}(\text{PO}_4)/\text{C}$	Colloidal crystal template method	In 3.0-4.8V, 169 mAhg^{-1} with 87.5 % capacity retention after 100 cycles at 1 C	39
$\text{Li}_3\text{V}_{1.85}\text{Nd}_{0.15}(\text{PO}_4)/\text{C}$	Sol-gel reaction	In 3.0-4.8V, showing an initial capacity of 162 mAhg^{-1} with a capacity retention of about 86.6% at 0.5C after 50 cycles	23
$\text{Li}_3\text{V}_{1.97}\text{Tm}_{0.03}(\text{PO}_4)_3/\text{C}$	Solid-state reaction	In 3.0-4.8V, showing an initial capacity of 181.2 mAhg^{-1} , with a capacity retention of 92.4% after 30 cycles.	40
$\text{Li}_3\text{V}_{1.98}\text{La}_{0.02}(\text{PO}_4)/\text{C}$	microwave-assisted carbothermal reduction	In 3.0-4.8V, 168.8 mAhg^{-1} with 93% capacity retention after 30 cycles at 0.2C	42
$\text{Li}_3\text{V}_{1.96}\text{La}_{0.04}(\text{PO}_4)/\text{C}$	Sol-gel assisted low temperature reaction	In 3.0-4.8V, 171 mAhg^{-1} with 94% capacity retention after 100 cycles at 0.2C	This work

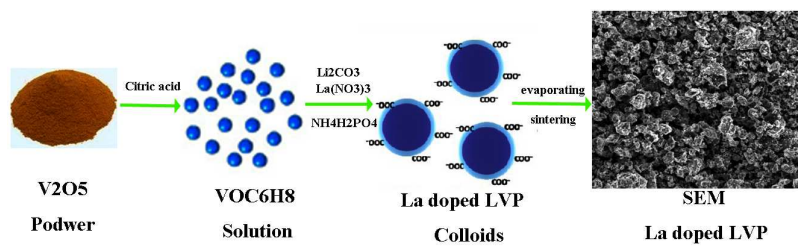


Fig. 1. The processes of the La doped $\text{Li}_3\text{V}_2(\text{PO}_4)_3/\text{C}$ composites

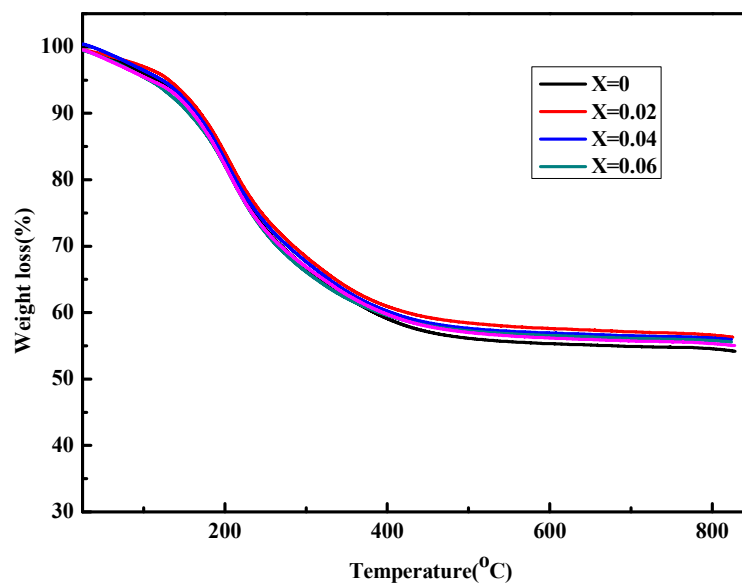


Fig. 2. TG curve for the dry gel precursor of $\text{Li}_3\text{V}_{2-x}\text{La}_x(\text{PO}_4)_3/\text{C}$ ($x=0, 0.02, 0.04, 0.06$) under N_2 flow at a heating rate of $10^{\circ}\text{C}/\text{min}$.

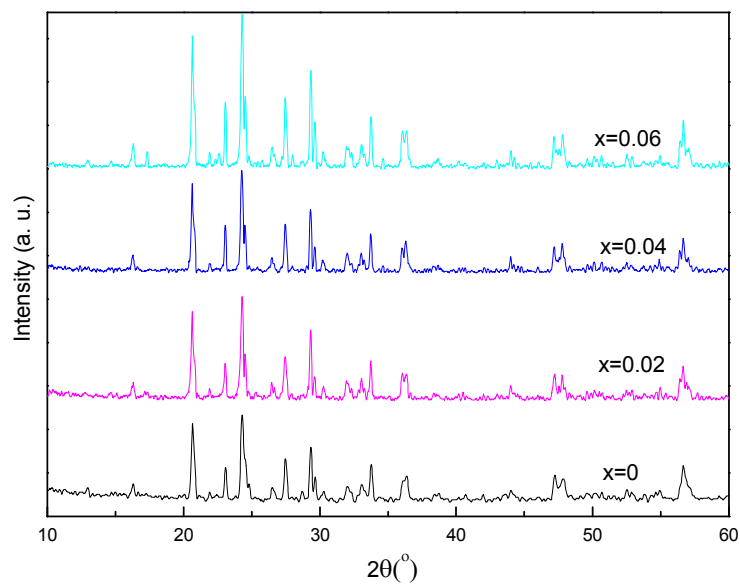


Fig. 3. XRD patterns of the $\text{Li}_3\text{V}_{2-x}\text{La}_x(\text{PO}_4)_3/\text{C}$ ($x=0, 0.02, 0.04, 0.06$) samples as a function of La ion doping

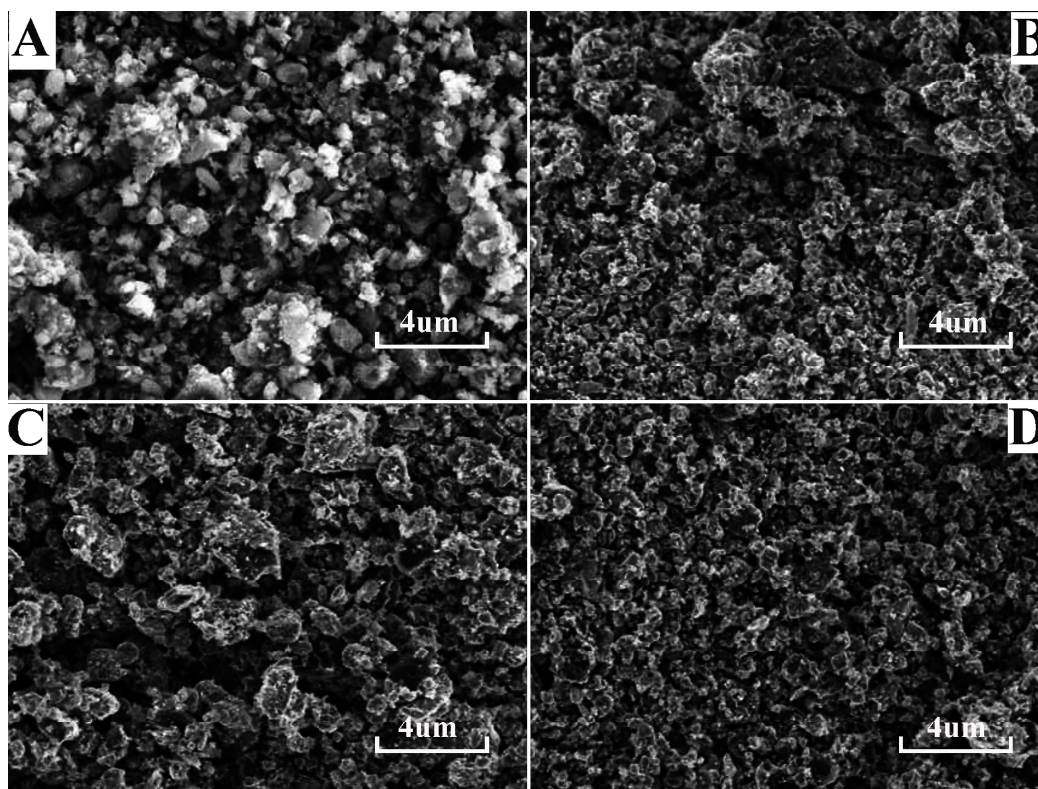


Fig. 4 SEM images of $\text{Li}_3\text{V}_{2-x}\text{La}_x(\text{PO}_4)_3/\text{C}$ samples with different La contents: (a) $x=0$, (b) $x=0.02$; (c) $x=0.04$; (d) $x=0.06$;

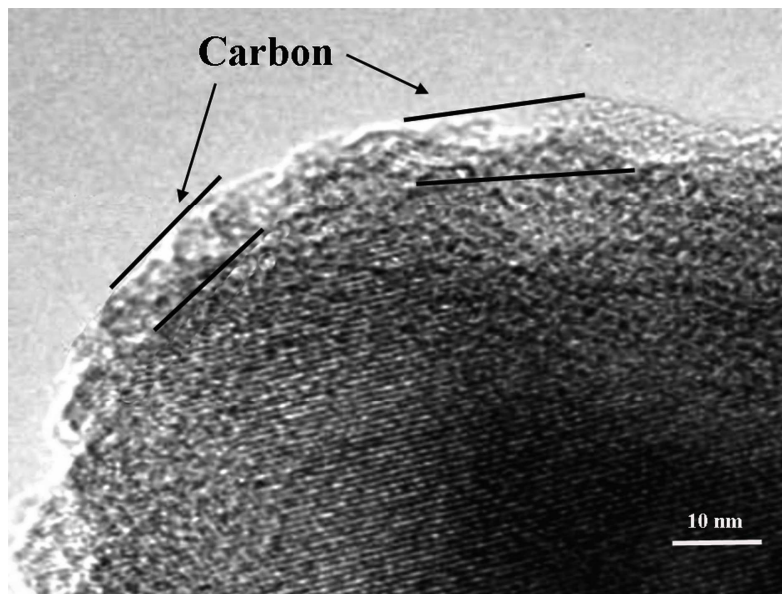


Fig. 5 TEM images of $\text{Li}_3\text{V}_{1.96}\text{La}_{0.04}(\text{PO}_4)_3/\text{C}$.

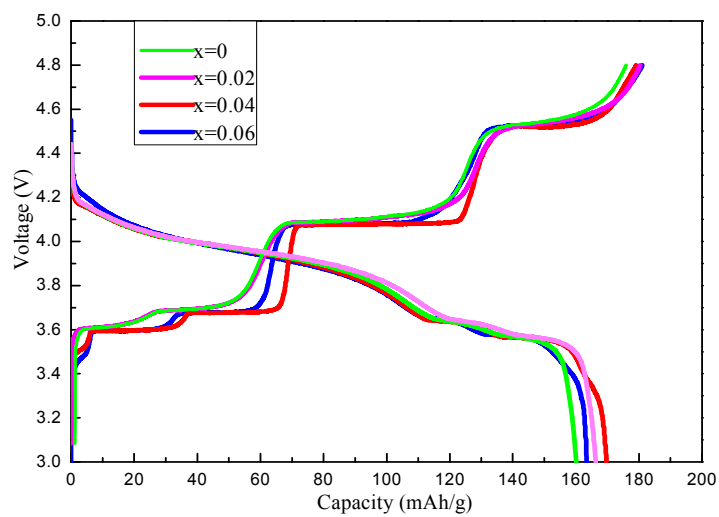


Fig. 6. Initial charge-discharge profiles of $\text{Li}_3\text{V}_{2-x}\text{La}_x(\text{PO}_4)_3/\text{C}$ ($x=0, 0.02, 0.04, 0.06$) at the 0.2C rate in the voltage of 3.0V- 4.8V.

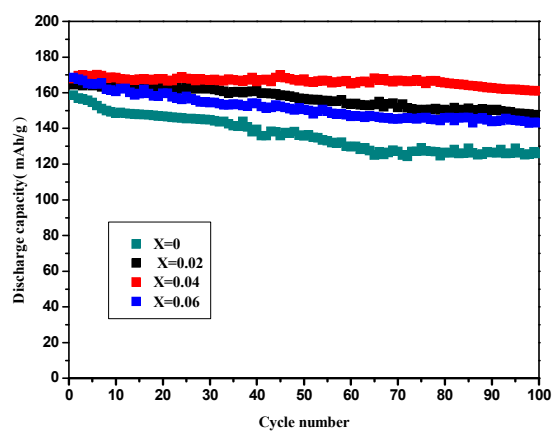


Fig. 7. Cycling performance of $\text{Li}_3\text{V}_{2-x}\text{La}_x(\text{PO}_4)_3/\text{C}$ ($x=0, 0.02, 0.04, 0.06$) at 0.2C discharge rate between 3.0V and 4.8V.

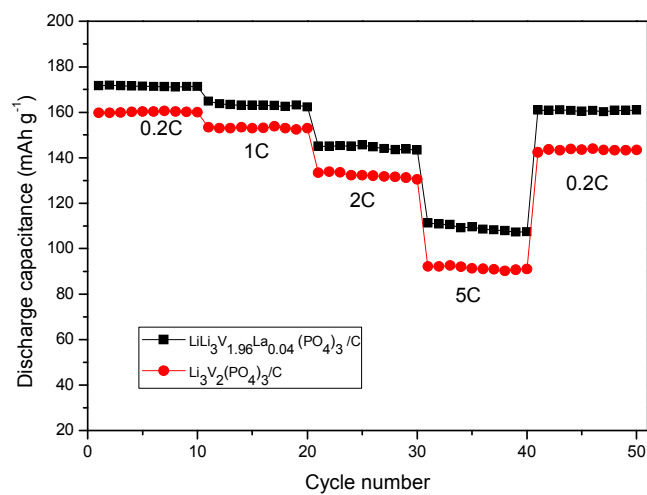


Fig. 8. Cycling performance of $\text{Li}_3\text{V}_2(\text{PO}_4)_3/\text{C}$ and $\text{Li}_3\text{V}_{1.96}\text{La}_{0.04}(\text{PO}_4)_3/\text{C}$ at different discharge rate of 0.2C, 1C, 2C, and 5C, respectively, between 3.0V-4.8V.

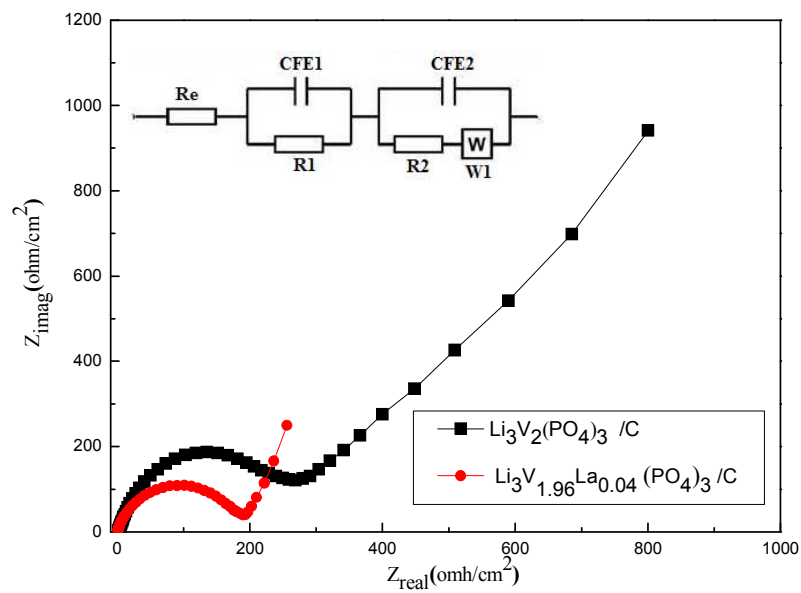


Fig. 9. Impedance spectra of the $\text{Li}_3\text{V}_2(\text{PO}_4)_3/\text{C}$ and $\text{Li}_3\text{V}_{1.96}\text{La}_{0.04}(\text{PO}_4)_3/\text{C}$ composites. Inset: Equivalent circuit corresponding to the impedance diagrams.